Supplemental Figure S1. Dendrites of v'ada neurons cover segmental boundaries in a complete and redundant manner.

Two neighboring v'ada neurons were labeled with EGFP ad mCitrine respectively by the Flybow system.

Supplemental Figure S2. Dendritic fields of wild-type and *Wnt5* mutant v'ada neurons.

(A, B) Dendritic fields of v'ada neurons in wild-type (A) and *Wnt5* mutant (B) abdomens.

(C, D) Quantification of the dendritic field size (C, $p = 0.628$) and the field width (D, $p = 0.434$) of v'ada neurons in wild-type and *Wnt5* mutants.

(E, F) Quantification of the total dendritic length (E, $p = 0.59$) and the number of branch points outside of sternites (F, $p = 0.38$) in wild-type and *Wnt5* mutant neurons. Error bars indicate standard error of the mean. n.s. > 0.05; unpaired Student's *t* test.

(G, H) Quantification of the number of bristles on a sternite (G, $p = 0.63$) and the size of sternites (H, $p = 0.19$) in wild-type and *Wnt5* mutants. Error bars indicate standard error of the mean. n.s. > 0.05; unpaired Student's *t* test.

(I, J) Relative position of v'ada dendrites and ECM in wild-type (I-I''') and *Wnt5* (J-J''') 5-day adults. Dendrites and ECM are visualized with *ppk*-CD4tdTom and vkg::GFP, respectively. Scale bar, 50 mm. Live imaging of dendrite-ECM interaction was performed as described previously (Han et al., 2012) with modifications. Briefly, image stacks were acquired using a Leica TCS SP8 confocal microscope equipped with a 40x/1.30 NA oil objective at high resolution (1024x1024 pixel, 0.28 mm per pixel, 0.24-0.26 mm z step size). The image stacks were then processed using LAS AF software (Leica Microsystems) to construct x-z sections.

Supplemental Figure S3. Generation of Wnt5-EGFP constructs

(A) A schematic of the P[acman]-CH322-141N12. The genomic fragment inserted into this P[acman] vector is indicated by the black box.

(B) A strategy to generate the Wnt5-EGFP vector. Wnt5-EGFP-stop/Kmr cassette is introduced immediately downstream of the ATG start codon.

(C, D) Late pupal brains from control (C) and *Wnt5-EGFP* transgenic (D) flies stained with GFP antibodies. Wnt5-EGFP is expressed dominantly in the optic lobes. The outline of the optic lobe is highlighted with the white line. Me, medulla; MeN, medulla neurons. Scale bars, 50 μm.
(E) Wnt5-EGFP expression in abdominal epithelial cells. Representative images of Wnt5-EGFP expression in 2-day adults (left), and 5-day adults (right) are shown. Arrowheads indicate the ventral midline. Scale bars, 100 μm.

Supplemental Figure S4. Ectopic expression of Wnt5 restricts C4da dendrite growth in larval epithelial cells
(A, B) v'ada dendrites in *hh*-positive epidermal cells in control (A) and *hh*-Gal4 *UAS-Wnt5* (B) third instar larvae. v'ada dendrites are labeled with *ppk*-CD4tdTom (magenta) and *hh*-positive cells are labeled with GFP (green).
(A', B') Dendrites in *hh*-positive regions.
(C) Quantification of C4da dendrite length in control and Wnt5-expressing larvae. Error bars indicate standard error of the mean. n.s. > 0.05, *$p < 0.05$; unpaired Student's *t* test.
(D) Expression of *drl* in the third instar larvae.
(E) Wnt5-EGFP expression in third instar larvae. Arrowheads indicate the soma of v'ada neurons. Scale bars, 100 mm (A, E); 50 mm (D).

Supplemental Figure S5. Dendritic fields of *drl*, *Drl-2,* and *drl Drl-2 double mutant v'ada neurons.*
(A-D) Dendritic fields of *wild-type* (A), *drl* (B), *Drl-2* (C), and *drl Drl-2* (D) mutant v'ada neurons. Scale bars, 100 μm.
(E-H) Quantification of the dendritic field area (E, $p = 0.495$), the field width (F, $p = 0.155$), the total dendritic length (G, $p = 0.391$), and the number of branch points (H, $p = 0.197$) of wild-type, *drl, Drl-2, and drl Drl-2 double* mutant neurons. Error bars indicate standard error of the mean. The numbers below each bar indicate n values. n.s. > 0.05; one-way ANOVA.
(I, J) Quantification of the distance from ventral midline to the dendritic branch terminals (I) and the total dendritic length within single sternites (J) in v'ada neurons that express UAS-*drl*-shRNA, *UAS-Drl2-shRNA*, or both

UAS-drl-shRNA and *UAS-Drl2-shRNA*. *UAS-mCherry-shRNA* was used as a control. One-way ANOVA followed by Dunnett's test. *$p < 0.05$, **$p < 0.01$. All shRNA lines were obtained from the TRiP collection at Harvard Medical School: *mCherry-shRNA* (#35785), *drl-shRNA* (#29602), and *Drl-2-shRNA* (#25961).

Supplemental Figure S6. Drl and Drl-2 receptors function cell autonomously in v'ada neurons to specify ventral boundary

(A-D) Ventral views of of v'ada dendrites in wild-type control (A), *drl Drl-2* double mutants (B), *drl Drl-2* double mutants with *UAS-drl* transgene (C), and *drl Drl-2* double mutants with *UAS-Drl2* transgene (D). Scale bars, 50 μm.

Supplemental Figure S7. Localization pattern of Drl::GFP protein in v'ada dendrites

(A, B) A live confocal image of a v'ada neuron labeled with mCD8RFP at 1-day adult (A) and a schematic trace of a primary dendrite (B). Scale bar, 50 mm. The primary dendrite was divided into ten parts along proximal-distal axis for quantification of Drl::GFP distribution.

(C, D) A representative image of Drl::GFP localization in the medial part (C) and the distal (D) part of the primary dendrite. Scale bar, 10 mm.

(E) Quantification of Drl::GFP intensity in primary dendrites. Error bars indicate standard error of the mean (n = 4).

Supplemental Figure S8. Dendritic fields of trio mutant v'ada neurons

(A, B) Quantification of the dendritic field size (A) and the field width (B) of v'ada neurons in wild-type control, $trio^{E4.1}$, and $trio^{E4.1}$ with *UAS-trio* transgene MARCM clones.

(C, D) Quantification of the total dendritic length (C) and the number of branch points outside of sternites (D). Error bars indicate standard error of the mean. n.s. > 0.05, *$p < 0.05$; One-way ANOVA followed by Tukey's HSD test.

Supplemental Figure S9. Genetic interactions between *trio* and *Wnt5/drl* genes

(A-F) Ventral boundary phenotypes in the indicated genotypes. Bottoms are

tracings of the top images. Scale bars, 50 μm.
(G, H) Quantification of the distance from ventral midline to branch terminals (G) and the total dendritic length within single sternites (H). Error bars indicate standard error of the mean. The numbers below each bar indicate n values. *$p <$ 0.05, **$p < 0.01$.

Supplemental Figure S10. The effects of the dominant-negative Rho1 and Rac1 in the ventral boundary formation
(A-C) Rho1-DN, but not Rac1-DN, affects the ventral boundaries of v'ada dendrites. For temporal expression of the dominant negative Rho1 (Rho1-N19) or Rac1 (Rac1-N17) in the pupal/adult stage, we utilized the Flip-out technique (see Experimental procedures). Bottoms are tracings of the top images. Scale bars, 50 μm.
(D, E) Quantification of the distance from the ventral midline to branch terminals (D) and the total dendritic length within single sternites (E). Error bars indicate standard error of the mean. The numbers below each bar indicate n values. *$p <$ 0.05. In D, significance compared to control, *control* versus *UAS-Rho1-N19*, $p =$ 0.187; *control* versus *UAS-Rac1-N17*, $p = 0.545$, one-way ANOVA followed by Dunnett's test. In E, *control* versus *UAS-Rho1-DN*, $p = 0.030$; *control* versus *UAS-Rac1-N17*, $p = 0.998$, one-way ANOVA followed by Dunnett's test.
(F, G) Quantification of the total dendritic length (F, $p = 0.16$) and the number of branch points outside of sternites (G, $p = 0.11$) in *control* and *UAS-Rho1-N19* neurons. Error bars indicate standard error of the mean. n.s. > 0.05; unpaired Student's *t* test.

Supplemental Movie S1. Live images of adult C4da dendrites at the segmental boundaries.

Supplemental References

Barrett K, Leptin M, Settleman J. 1997. The Rho GTPase and a putative RhoGEF mediate a signaling pathway for the cell shape changes in

Drosophila gastrulation. *Cell* **91:** 905-915.

Billuart P, Winter CG, Maresh A, Zhao X, Luo L. 2001. Regulating axon branch stability: the role of p190 RhoGAP in repressing a retraction signaling pathway. *Cell* **107:** 195-207.

Buff E, Carmena A, Gisselbrecht S, Jiménez F, Michelson AM. 1998. Signalling by the *Drosophila* epidermal growth factor receptor is required for the specification and diversification of embryonic muscle progenitors. *Development* **125:** 2075-2086.

Callahan CA, Bonkovsky JL, Scully AL, Thomas JB. 1996. derailed is required for muscle attachment site selection in *Drosophila*. *Development* **122:** 2761-2767.

Chen CM, Struhl G. 1999. Wingless transduction by the Frizzled and Frizzled2 proteins of *Drosophila*. *Development* **126:** 5441-5452.

Chen Y, Struhl G. 1998. In vivo evidence that Patched and Smoothened constitute distinct binding and transducing components of a Hedgehog receptor complex. *Development* **125:** 4943-4948.

Cohen ED, Mariol MC, Wallace RM, Weyers J, Kamberov YG, Pradel J, Wilder EL. 2002. DWnt4 regulates cell movement and focal adhesion kinase during *Drosophila* ovarian morphogenesis. *Dev Cell* **2:** 437-448.

Gubb D, Green C, Huen D, Coulson D, Johnson G, Tree D, Collier S, Roote J. 1999. The balance between isoforms of the prickle LIM domain protein is critical for planar polarity in *Drosophila* imaginal discs. *Genes Dev* **13:** 2315-2327.

Holbrook S, Finley JK, Lyons EL, Herman TG. 2012. Loss of syd-1 from R7 neurons disrupts two distinct phases of presynaptic development. *J Neurosci* **32:** 18101-18111.

Hong W, Mosca TJ, Luo L. 2012. Teneurins instruct synaptic partner matching in an olfactory map. *Nature* **484:** 201-207.

Inaki M, Yoshikawa S, Thomas JB, Aburatani H, Nose A. 2007. Wnt4 is a local repulsive cue that determines synaptic target specificity. *Curr Biol* **17:** 1574-1579.

Jones KH, Liu J, Adler, PN. 1996. Molecular analysis of EMS-induced frizzled

mutations in *Drosophila* melanogaster. *Genetics* **142:** 205-215.

Kidd T, Brose K, Mitchell KJ, Fetter RD, Tessier-Lavigne M, Goodman CS, Tear G. 1998. Roundabout controls axon crossing of the CNS midline and defines a novel subfamily of evolutionarily conserved guidance receptors. *Cell* **92:** 205–215.

Kolodziej PA, Timpe LC, Mitchell KJ, Fried SR, Goodman CS, Jan LY, Jan YN. 1996. frazzled encodes a *Drosophila* member of the DCC immunoglobulin subfamily and is required for CNS and motor axon guidance. *Cell* **87:** 197-204.

Kozopas KM, Samos CH, Nusse R. 1998. DWnt-2, a *Drosophila* Wnt gene required for the development of the male reproductive tract, specifies a sexually dimorphic cell fate. *Genes Dev* **12:** 1155-1165.

Labrador JP, O'keefe D, Yoshikawa S, McKinnon RD, Thomas JB., Bashaw GJ. 2005. The homeobox transcription factor even-skipped regulates netrin-receptor expression to control dorsal motor-axon projections in *Drosophila*. *Curr Biol* **15:** 1413-1419.

Lahaye LL, Wouda RR, de Jong AW, Fradkin, LG, Noordermeer, J.N. 2012. WNT5 interacts with the Ryk receptors doughnut and derailed to mediate muscle attachment site selection in *Drosophila* melanogaster. *PLoS One* **7:** e32297.

McElwain, MA, Ko DC, Gordon MD, Fyrst H, Saba JD, Nusse R. 2011. A suppressor/enhancer screen in *Drosophila* reveals a role for wnt-mediated lipid metabolism in primordial germ cell migration. *PLoS One* **6:** e26993.

Michelson AM, Gisselbrecht S, Zhou Y, Baek KH, Buff, EM. 1998. Dual functions of the heartless fibroblast growth factor receptor in development of the *Drosophila* embryonic mesoderm. *Dev Genet* **22:** 212-229.

Neisch AL, Formstecher E, Fehon RG. 2013. Conundrum, an ARHGAP18 orthologue, regulates RhoA and proliferation through interactions with Moesin. *Mol Biol Cell* **24:** 1420-1433.

Nellen D, Affolter M, Basler K. 1994. Receptor serine/threonine kinases implicated in the control of Drosophila body pattern by decapentaplegic. *Cell* **78:** 225-237.

Nüsslein-Volhard C, Wieschaus E, Kluding H. 1984. Mutations affecting the pattern of the larval cuticle in *Drosophila melanogaster. Roux's Arch Dev Biol* **193:** 267-282.

O'Reilly AM, Ballew AC, Miyazawa B, Stocker H, Hafen E, Simon MA. 2006. Csk differentially regulates Src64 during distinct morphological events in *Drosophila* germ cells. *Development* **133:** 2627-2638.

Pappu KS, Morey M, Nern A, Spitzweck B, Dickson BJ, Zipursky SL. 2011. Robo-3-mediated repulsive interactions guide R8 axons during *Drosophila* visual system development. *Proc Natl Acad Sci USA* **108:** 7571-7576.

Perrimon N, Mahowald AP. 1987. Multiple functions of segment polarity genes in *Drosophila. Dev Biol* **119:** 587-600.

Sanny J, Chui V, Langmann C, Pereira C, Zahedi B, Harden N. 2006. *Drosophila* RhoGAP68F is a putative GTPase activating protein for RhoA participating in gastrulation. *Dev Genes Evol* **216:** 543-550.

Schimmelpfeng K, Gögel S, Klämbt C. 2001. The function of leak and kuzbanian during growth cone and cell migration. *Mech Dev* **106:** 25-36.

Seeger M, Tear G, Ferres-Marco D, Goodman CS. 1993. Mutations affecting growth cone guidance in *Drosophila*: genes necessary for guidance toward or away from the midline. *Neuron* **10:** 409-426.

Shindo M, Wada H, Kaido M, Tateno M, Aigaki T, Tsuda L, Hayashi S. 2008. Dual function of Src in the maintenance of adherens junctions during tracheal epithelial morphogenesis. *Development* **135:** 1355-1364.

Twombly V, Bangi E, Le V, Malnic B, Singer M., Wharton KA. 2009. Functional analysis of saxophone, the *Drosophila* gene encoding the BMP type I receptor ortholog of human ALK1/ACVRL1 and ACVR1/ALK2. *Genetics* **183:** 563-579.

Wehrli M, Dougan ST, Caldwell K, O'Keefe L, Schwartz S, Vaizel-Ohayon D, Schejter E, Tomlinson A, DiNardo S. 2000. arrow encodes an LDL-receptor-related protein essential for Wingless signalling. *Nature* **407:** 527-530.

Winberg ML, Mitchell KJ, Goodman CS. 1998. Genetic analysis of the

mechanisms controlling target selection: complementary and combinatorial functions of netrins, semaphorins, and IgCAMs. *Cell* **93,** 581-591.

Wolff T, Rubin GM. 1998. Strabismus, a novel gene that regulates tissue polarity and cell fate decisions in *Drosophila*. *Development* **125:** 1149-1159.

Yoshikawa S, McKinnon RD, Kokel M, Thomas JB. 2003. Wnt-mediated axon guidance via the *Drosophila* Derailed receptor. *Nature* **422:** 583-588.

Zheng X, Wang J, Haerry TE, Wu AY, Martin J, O'Connor MB, Lee CH, Lee T. 2003. TGF-beta signaling activates steroid hormone receptor expression during neuronal remodeling in the *Drosophila* brain. *Cell* **112:** 303-315.

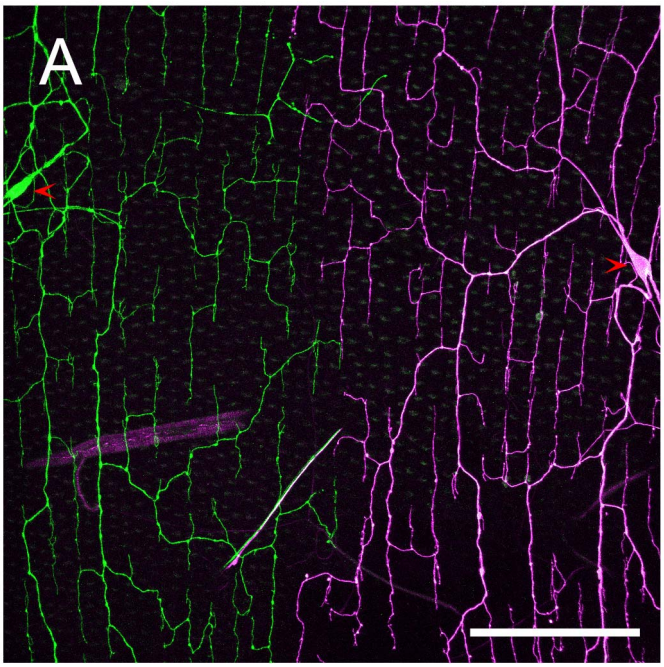
A

Yasunaga_FigS2

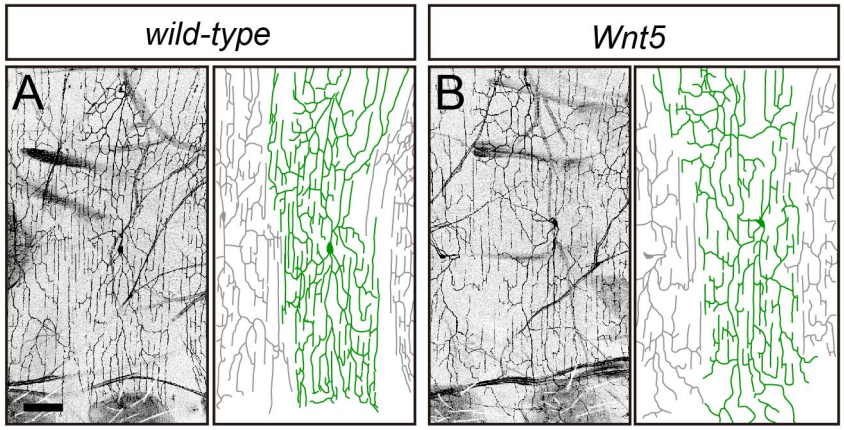

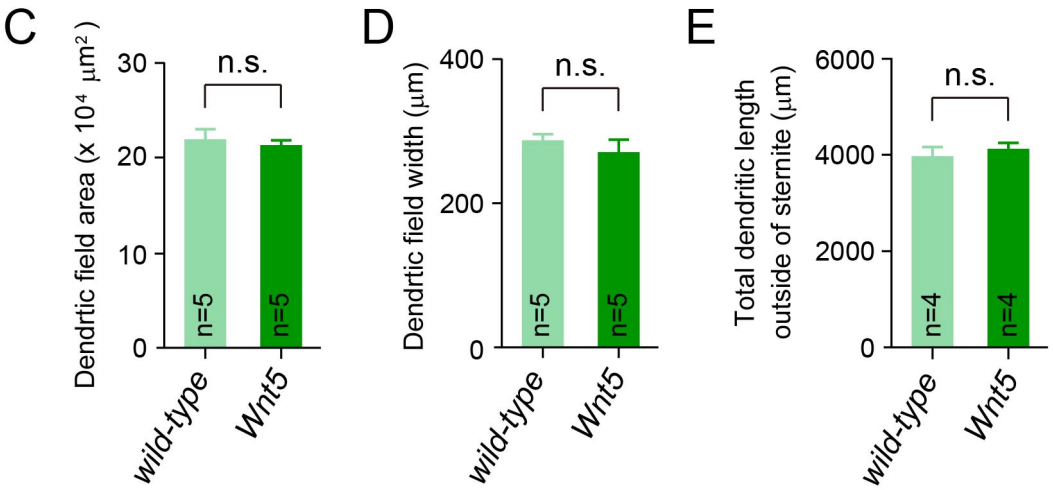

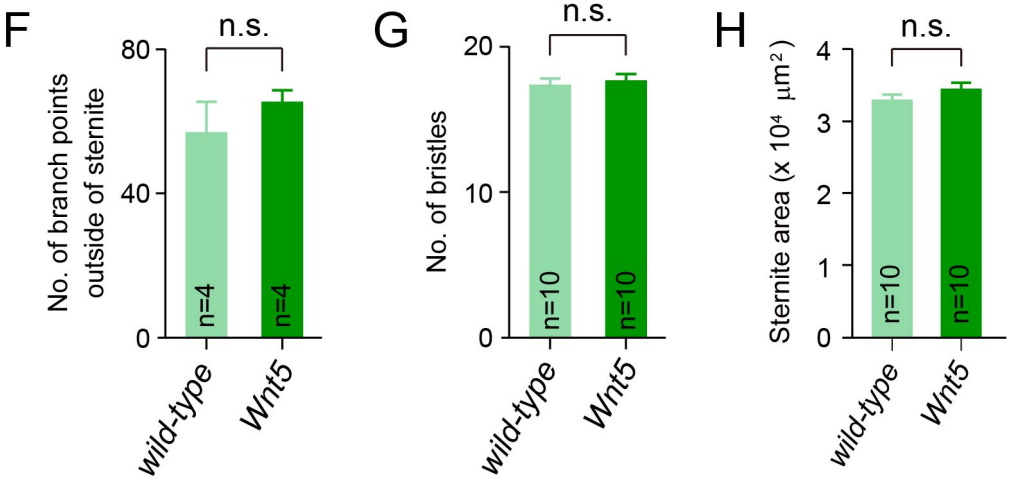

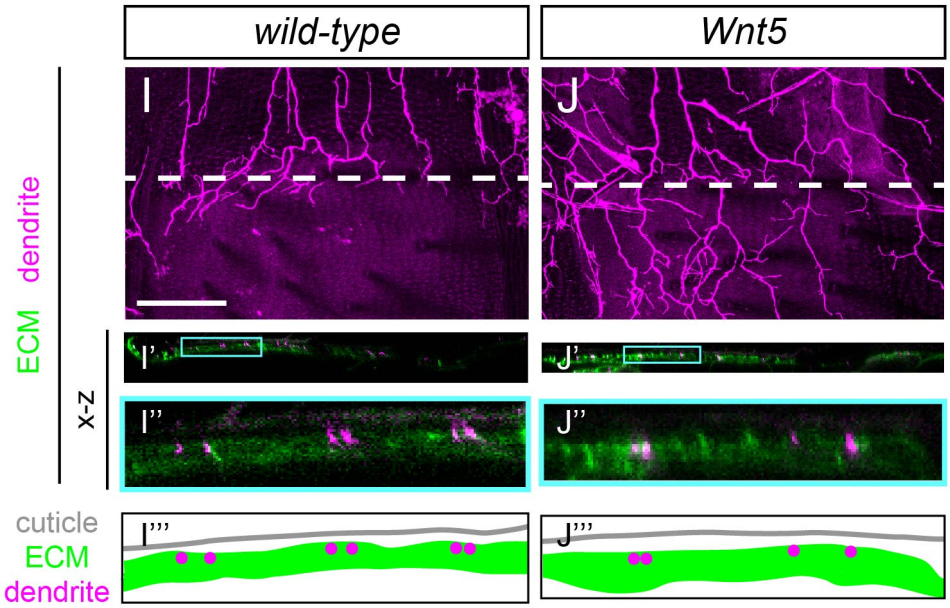

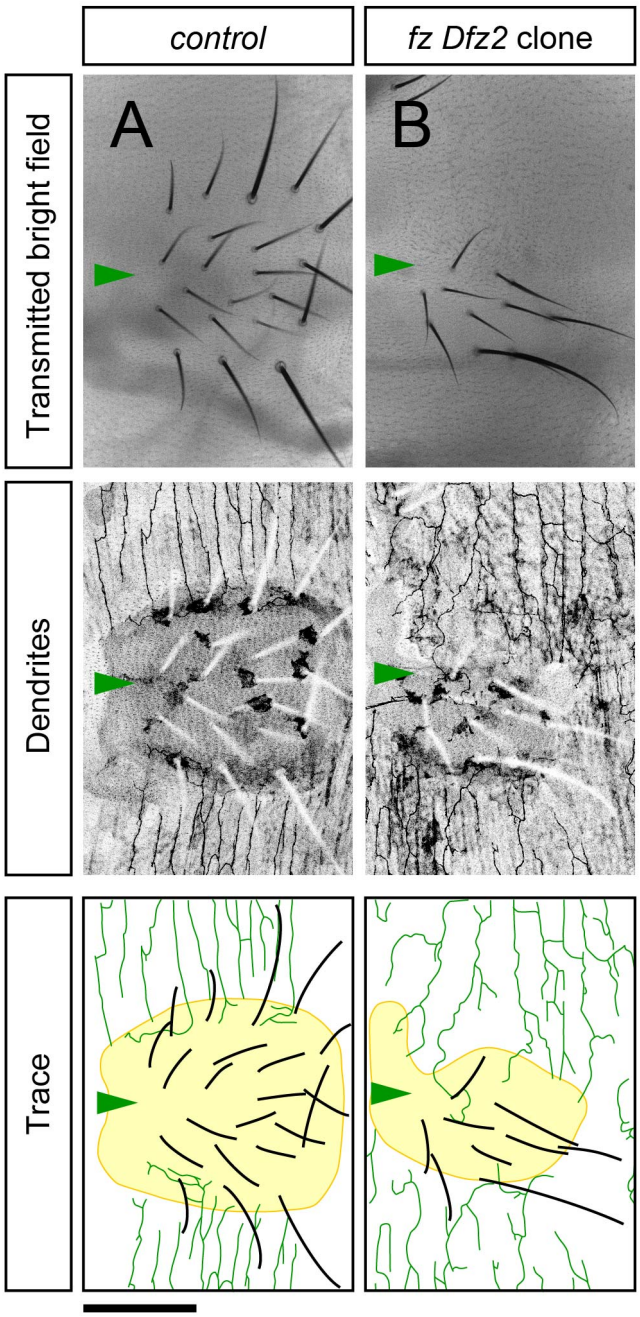
control
fz Dfz2 clone
Transmitted bright field
Dendrites
Trace
A
B

Yasunaga_FigS4

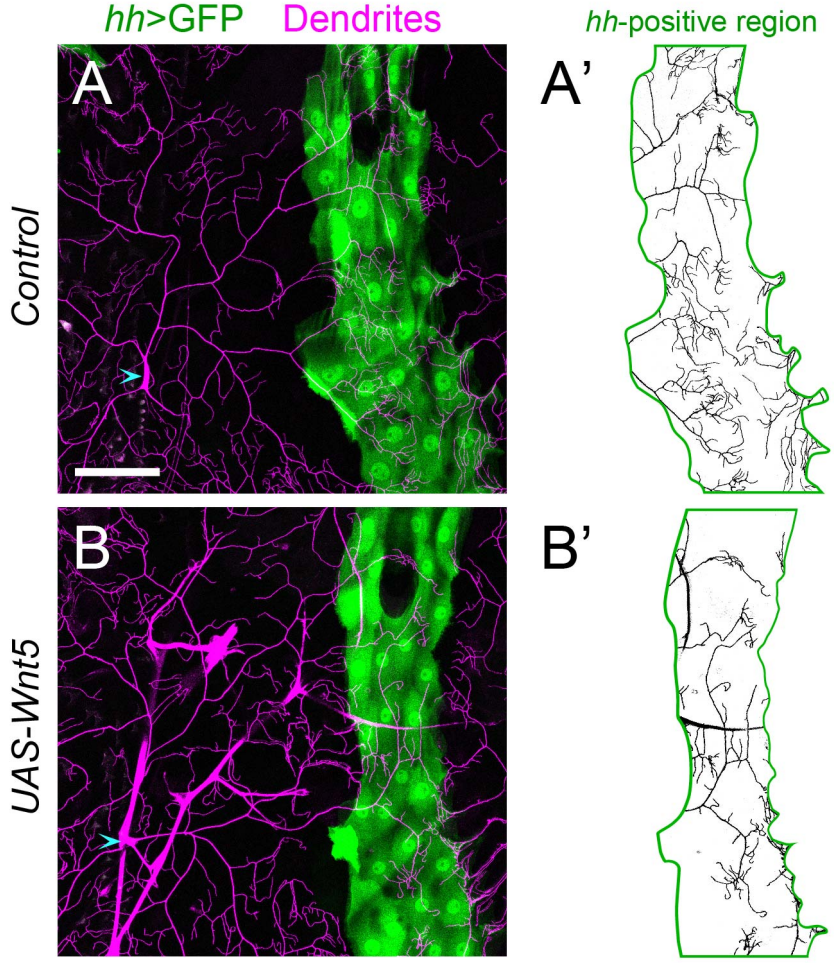

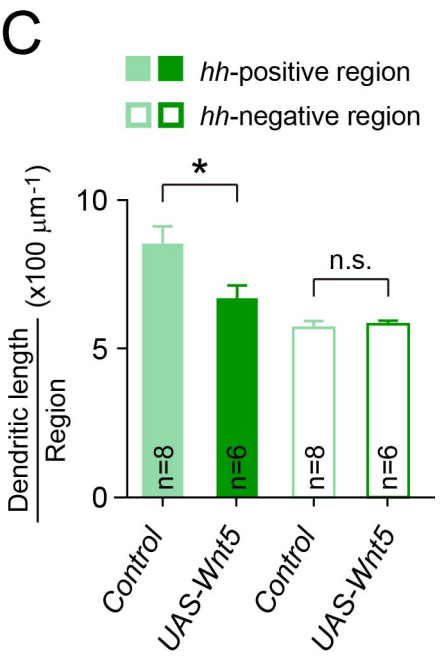

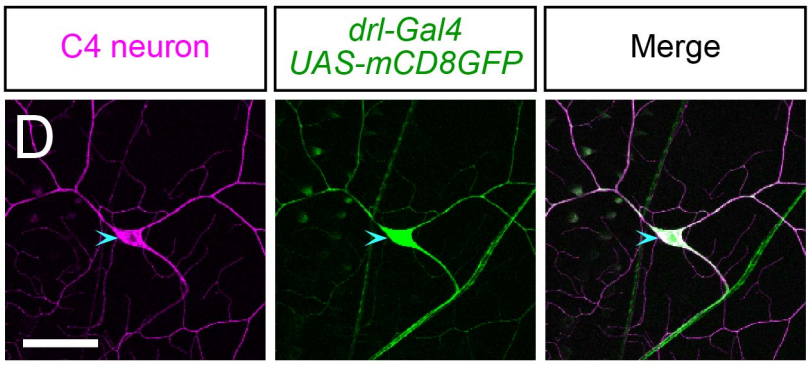

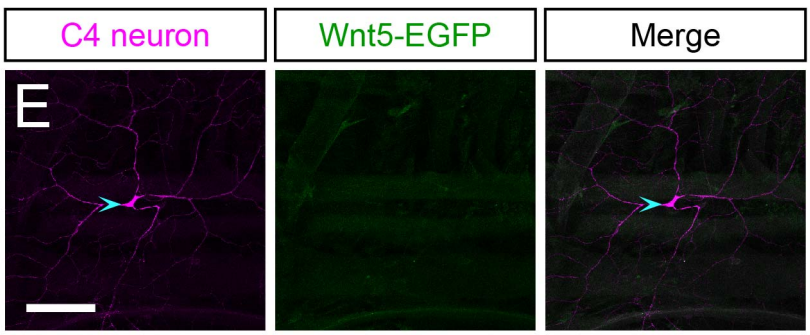

Yasunaga_Fig5

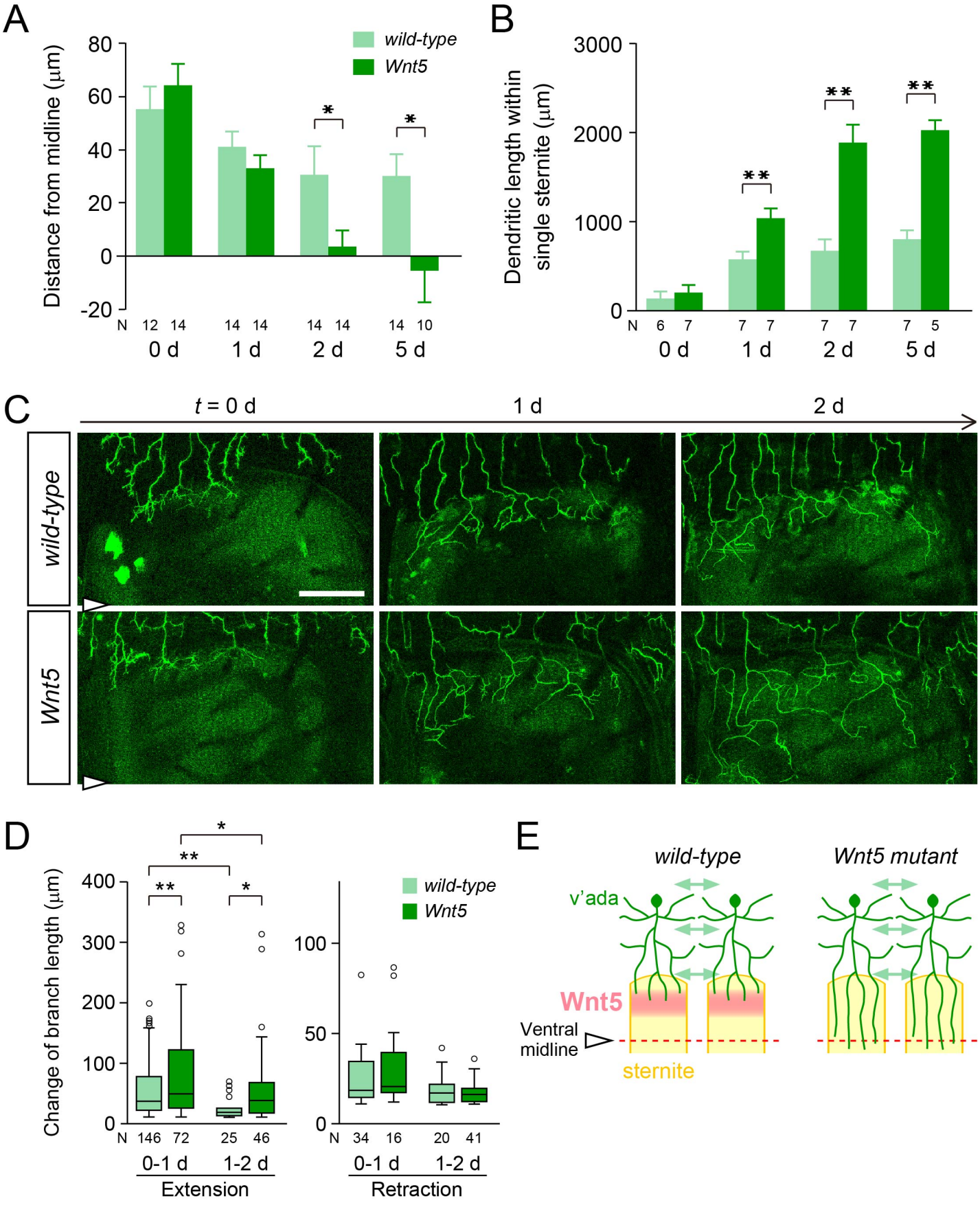

Yasunaga_FigS6

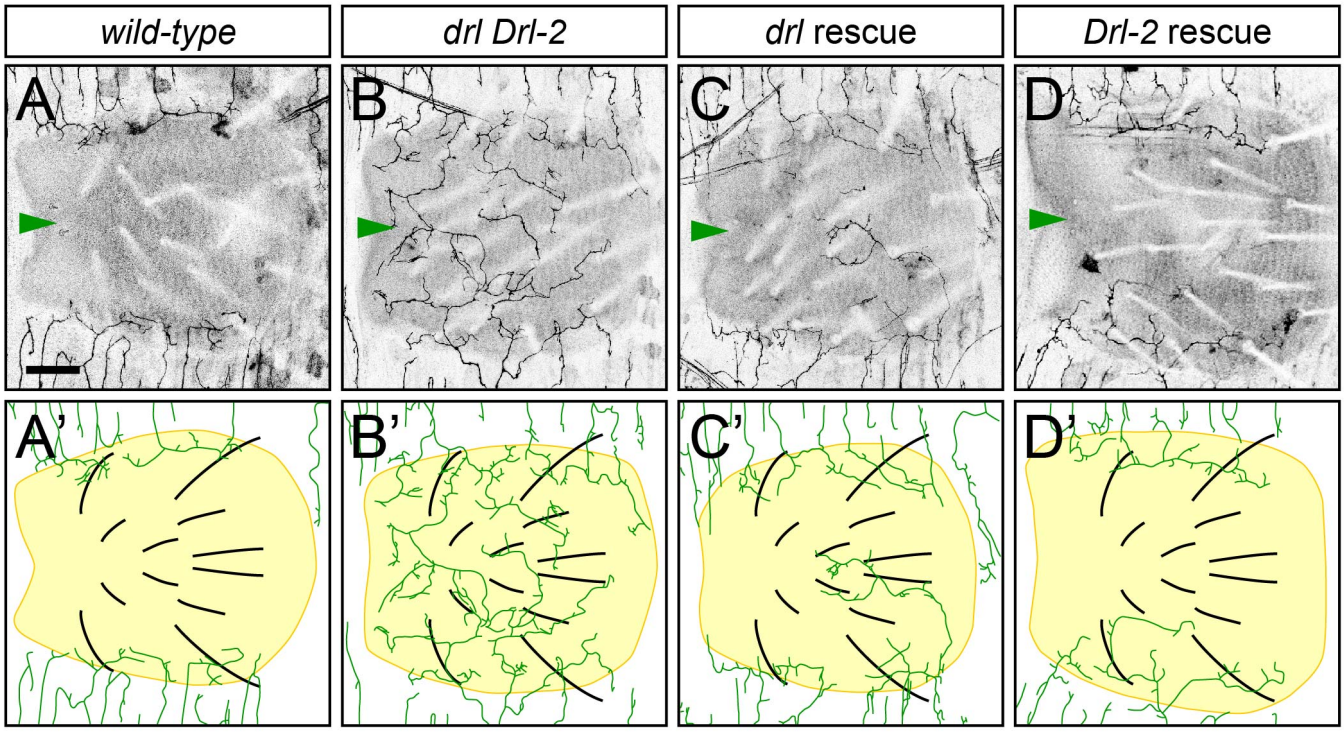

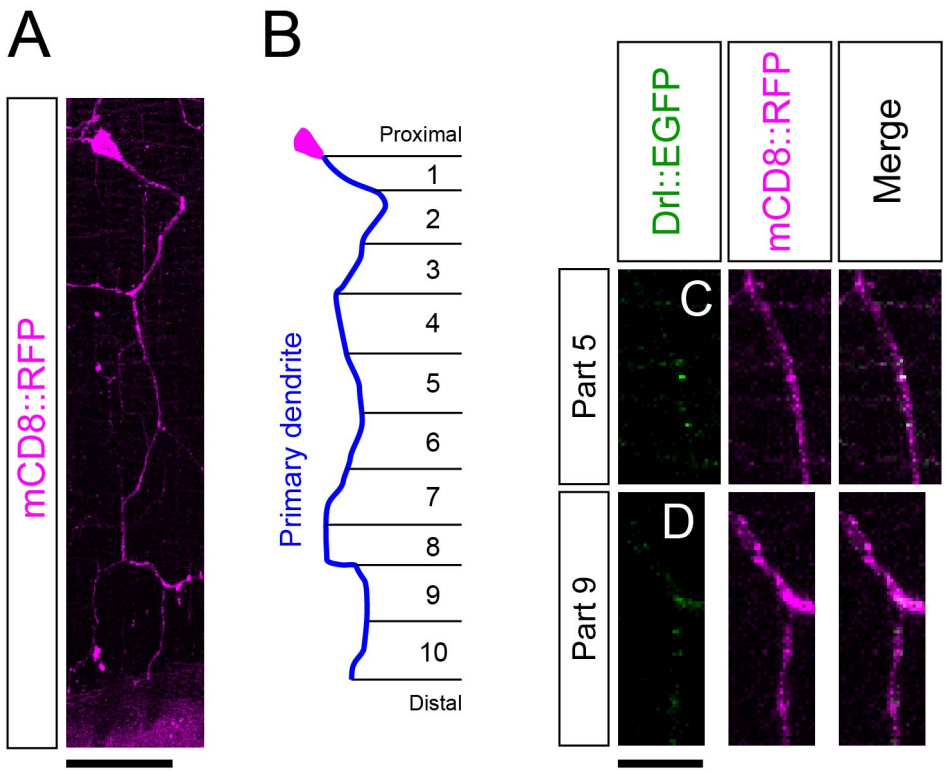
A
mCD8::RFP
B
Proximal
1
2
3
4
5
6
7
8
9
10
Distal
Primary dendrite
Drl::EGFP
mCD8::RFP
Merge
Part 5
C
Part 9
D

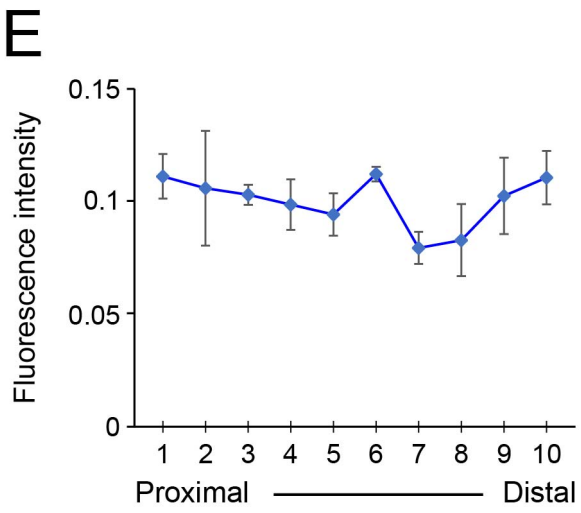
E
Fluorescence intensity
0.15
0.1
0.05
0
1 2 3 4 5 6 7 8 9 10
Proximal
Distal

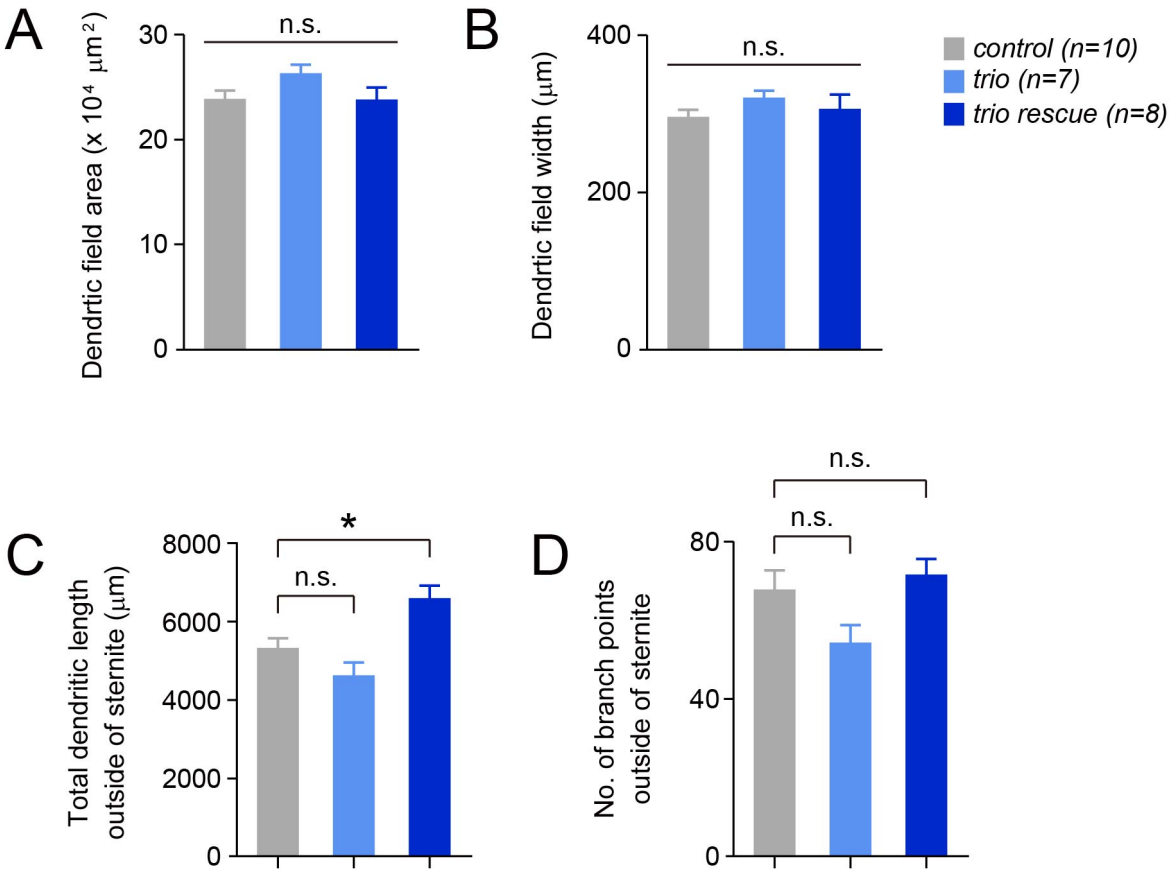
A
Dendrtic field area (x 10⁴ μm²)
30
20
10
0
n.s.
B
Dendrtic field width (μm)
400
200
0
n.s.
control (n=10)
trio (n=7)
trio rescue (n=8)
C
Total dendritic length outside of sternite (μm)
8000
6000
4000
2000
0
*
n.s.
D
No. of branch points outside of sternite
80
40
0
n.s.
n.s.

Yasunaga_FigS9

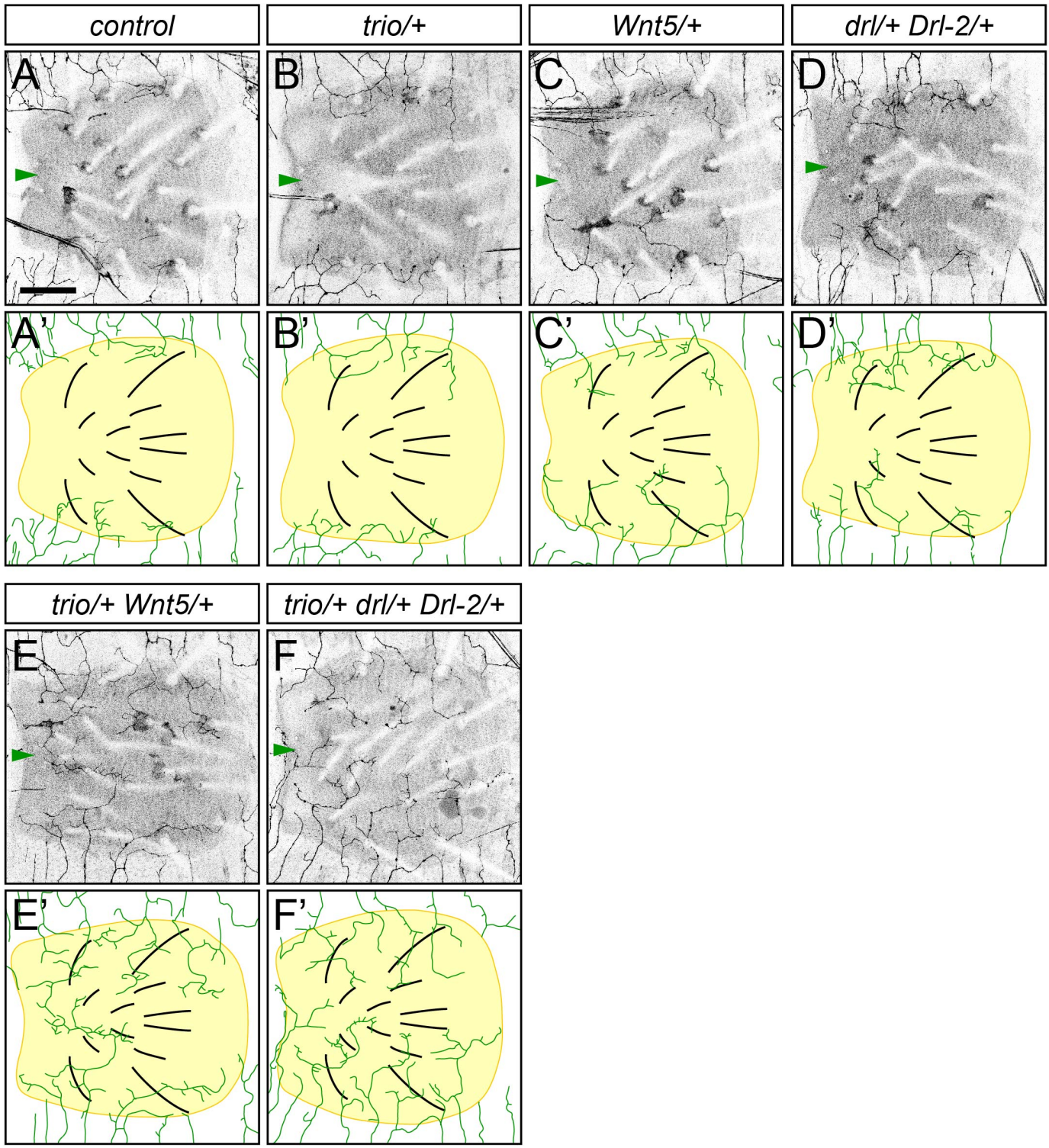

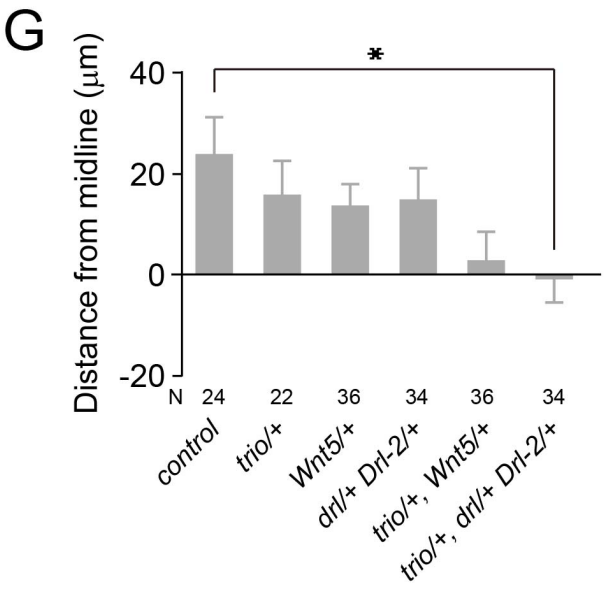

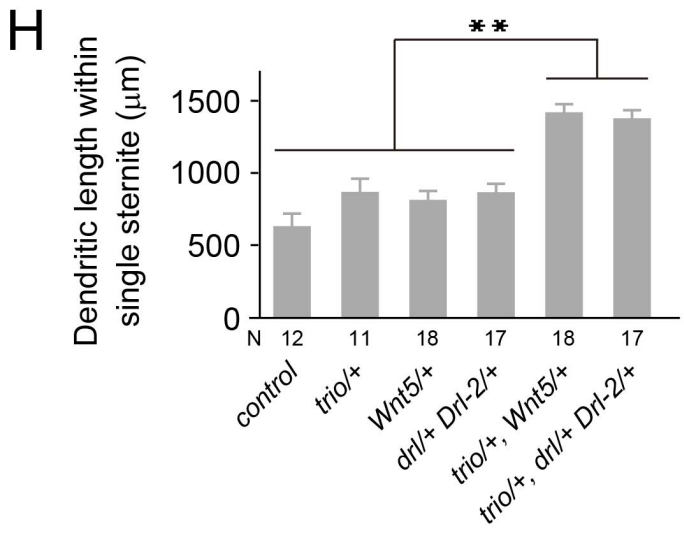

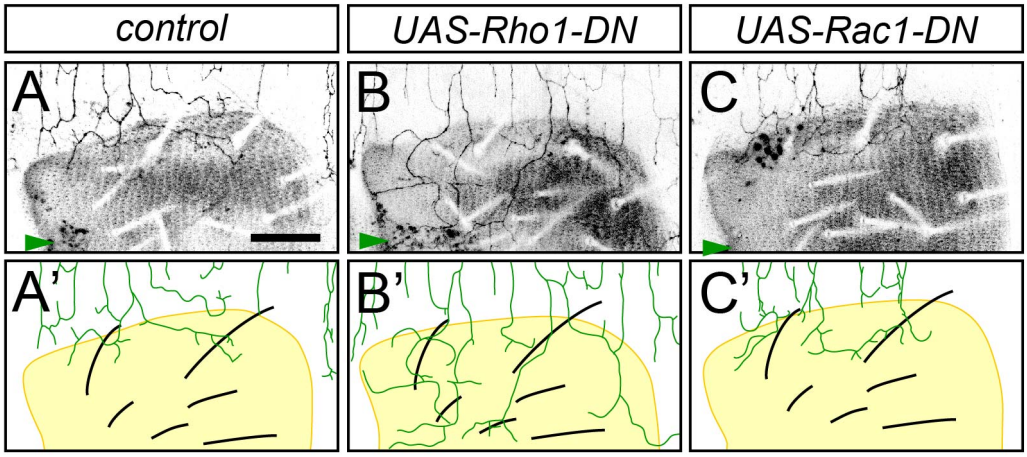
control
UAS-Rho1-DN
UAS-Rac1-DN
A
B
C
A'
B'
C'

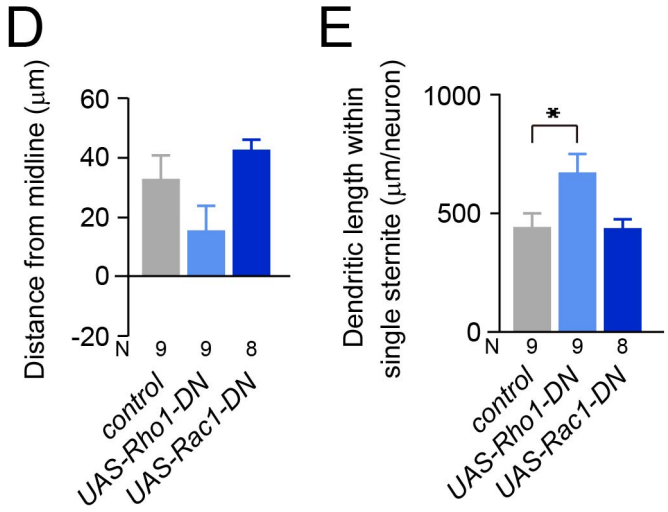
D
Distance from midline (μm)
60
40
20
0
-20
N 9 9 8
control
UAS-Rho1-DN
UAS-Rac1-DN
E
Dendritic length within single sternite (μm/neuron)
1000
500
0
*
N 9 9 8
control
UAS-Rho1-DN
UAS-Rac1-DN

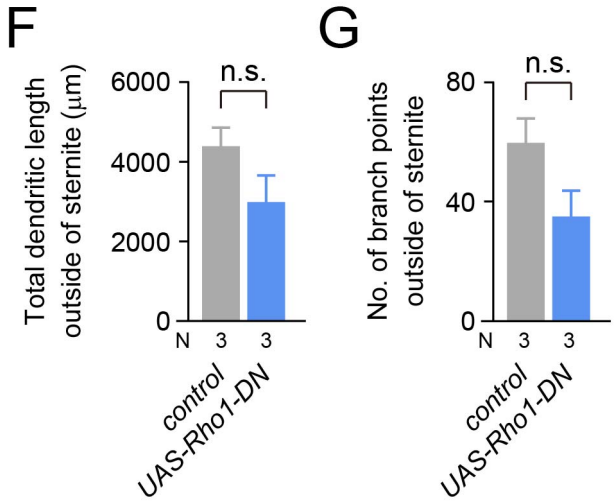
F
Total dendritic length outside of sternite (μm)
6000
4000
2000
0
n.s.
N 3 3
control
UAS-Rho1-DN
G
No. of branch points outside of sternite
80
40
0
n.s.
N 3 3
control
UAS-Rho1-DN

Supplementary Table S1
Boundary phenotypes of secreted molecules and receptors tested.

Gene name	Assay used for analysis of boundary formation	Alleles or UAS lines used	Defects in boundary formation[a]	Source
Wnt2	heteroallelic combination	*O / Df(2R)BSC408*	−	Kozopas et al., 1998
Wnt4	heteroallelic combination	*EMS23 / C1*	−	Cohen et al., 2002
Wnt5/Wnt3	homozygote	*D7*	+++	Yoshikawa et al., 2003
Wnt6	RNAi[b]	*BL30493*	−	TRiP line, VALIUM10
WntD/Wnt8	RNAi[b]	*BL28947*	−	TRiP line, VALIUM10
Wnt10	RNAi[b]	*BL31989*	−	TRiP line, VALIUM10
wg	not tested			
fz fz2[c]	MARCM	*HS1, C1*	−	Jones et al., 1996 Chen and Struhl, 1999
fz3	RNAi[d]	*BL44468*	−	TRiP, VALIUM22
fz4	homozygote	*3-1*	−	McElwain et al., 2011
arr	MARCM	*2*	−	Wehrli et al., 2000
Ror	homozygote	*271*[e]	−	This study
dnt	homozygote	*42.3*	−	Lahaye et al., 2012
drl	homozygote	*R343*	+	Callahan et al., 1996
Drl2	homozygote	*E124*	++	Inaki et al., 2007
drl Drl2	homozygote	*R343, E124*	+++	Callahan et al., 1996 Inaki et al., 2007
NetA NetB	homozygote	*Df(1)T9B118*	−	Winberg et al., 1998
fra	heteroallelic combination	*3 / 4*	−	Kolodziej et al., 1996
fra	RNAi[d]	*BL40826*	−	TRiP line, VALIUM20
unc-5	MARCM	*8*	−	Labrador et al., 2005
Robo	MARCM	*GA285*	+	Kidd et al., 1998
Robo2	homozygote	*1*	−	Schimmelpfeng et al., 2001
Robo3	homozygote	*3*	−	Pappu et al., 2011
ephrin	RNAi[d]	*BL34614*	+	TRiP line, VALIUM20
Eph	RNAi[d]	*BL39066*	−	TRiP line, VALIUM20
plexA	RNAi[d]	*BL30483*	−	TRiP line, VALIUM10
plexB	RNAi[d]	*BL28911*	−	TRiP line, VALIUM10
babo	MARCM	*9*	N.A.[f]	Zheng et al., 2003
tkv	MARCM	*8*	N.A.[g]	Nellen et al., 1994
sax	MARCM	*4*	−	Twombly et al., 2009
put	RNAi[d]	*BL39025*	−	TRiP line, VALIUM20
wit	RNAi[d]	*BL41906*	−	TRiP line, VALIUM20
smo	MARCM	*3*	+	Chen and Struhl, 1998
ptc	MARCM	*IIC*	−	Nüsslein-Volhard et al., 1984
ptc	RNAi[d]	*BL55686*	−	TRiP line, VALIUM20
Egfr	Dominant-negative form[h]	*BL5364*	−	Buff et al., 1998
btl	RNAi[d]	*BL43544*	−	TRiP line, VALIUM20
htl	Dominant-negative form[h]	*BL5366*	−	Michelson et al., 1998
Ten-a	homozygote	*Df(1)Ten-a*	−	Hong et al., 2012
Ten-a	RNAi[d]	*BL29439*	−	TRiP line, VALIUM10
Ten-m	RNAi[d]	*BL29390*	−	TRiP line, VALIUM10

[a]+++, strong; ++, moderate; +, weak; -, none
[b]The UAS-RNAi stocks were driven by *tub-GAL4, ppk-CD4-tdTomato*.
[c]We generated MARCM clones of C4da neurons doubly mutant for fz and fz2.
[d]The UAS-RNAi stocks were driven by *ppk-GAL4, UAS-mCD8GFP, UAS-dcr2*.
[e]*Ror*^{271} allele was generated by imprecise excision of the P-element {EP}G8235 inserted upstream of the transcription start site. This allele removes 2.9 kb (genomic region 2L:10,251,809-10,254,702) including the whole *Ror* coding region and a part of the CG5676 3' UTR.
[f]Dendrites were misdirected ventrally in *babo* MARCM clones.
[g]Total dendritic length and dendritic field area were severly reduced.
[h]All UAS-dominant negative stocks were driven by *ppk-GAL4, UAS-mCD8GFP*.
At least 3 neurons for each genotype were analyzed.

Supplementary Table S2
Boundary phenotypes of non-canonical Wnt signaling components tested. Yasunaga_Table S2

Gene name	Assay used for analysis of boundary formation	Alleles or UAS lines used	Defects in boundary formation	Source
PCP pathway				
fz	MARCM	*HS1*	−	Jones et al., 1996
dsh	RNAi[a]	*BL31306*	−	TRiP line, VALIUM1
dsh	homozygote	*1*	−	Perrimon and Mahowald, 1987
Vang	RNAi[a]	*BL34354*	−	TRiP line, VALIUM20
Vang	homozygote	*stbm-6*	−	Wolff and Rubin, 1998
pk	RNAi[a]	*BL32413*	−	TRiP line, VALIUM20
pk	homozygote	*sple*	+	Gubb et al., 1999
pk	homozygote	*pk*	−	Gubb et al., 1999
pk	MARCM	*pk-sple-13*	−	Gubb et al., 1999
fmi	RNAi[a]	*BL35050*	−	TRiP line, VALIUM20
dgo	RNAi[a]	*BL35040*	−	TRiP line, VALIUM20
Src pathway				
Src42A	RNAi[a]	*BL44039*	−	TRiP line, VALIUM20
Src42A	Dominant-negative form[c]	*KYOTO109998*	N.A.[b]	Shindo et al., 2008
Src64B	homozygote	*KO*	−	O'Reilly et al., 2006
Wnt-Ca^{2+} pathway				
CamKI	RNAi[a]	*BL26726*	−	TRiP line, VALIUM10
CamKII	RNAi[a]	*BL29401*	−	TRiP line, VALIUM10
sl(PLCgamma)	RNAi[a]	*BL32385*	−	TRiP line, VALIUM20
PLC21C	RNAi[a]	*BL33719*	−	TRiP line, VALIUM20
norpA(PLCbeta)	RNAi[a]	*BL31197*	−	TRiP line, VALIUM1
bsk(JNK)	RNAi[a]	*BL32977*	−	TRiP line, VALIUM20
bsk(JNK)	Dominant-negative form[c]	*BL6409*	−	Bloomington

[a]The UAS-RNAi stocks were driven by *ppk-GAL4, UAS-mCD8GFP, UAS-dcr2*.

[b]Total dendritic length and dendritic field area were severly reduced.

[c]The UAS-dominant-negative transgene was driven by *ppk-GAL4, UAS-mCD8GFP.*

+, weak; -, none

At least 3 neurons for each genotype were analyzed.

Supplementary Table S3
Boundary phenotypes of RhoGEFs and RhoGAPs tested.

Gene name	Assay used for analysis of boundary formation	Alleles or UAS lines used	Defects in boundary formation	Source
RhoGAP				
syd-1	RNAi[a]	*BL32946*	+	TRiP line, VALIUM20
syd-1	heteroallelic combination	*CD / W46*	−	Holbrook et al., 2012
RhoGAP102A	RNAi[a]	*BL33425*	−	TRiP line, VALIUM20
RhoGAP15B	RNAi[a]	*BL42527*	N.A.[b]	TRiP line, VALIUM20
RhoGAP16F	RNAi[a]	*BL42541*	−	TRiP line, VALIUM20
RhoGAP19D	RNAi[a]	*BL32361*	−	TRiP line, VALIUM20
RhoGAP54D	RNAi[a]	*BL31144*	−	TRiP line, VALIUM1
RhoGAP5A	RNAi[a]	*BL31163*	−	TRiP line, VALIUM1
RhoGAP68F	RNAi[a]	*BL41990*	+	TRiP line, VALIUM20
RhoGAP68F	homozygote	*EY05896*	−	Sanny et al., 2006
RhoGAP71E	RNAi[a]	*BL32417*	−	TRiP line, VALIUM20
drich	RNAi[a]	*BL33391*	−	TRiP line, VALIUM20
Vilse	RNAi[a]	*BL35027*	−	TRiP line, VALIUM20
RhoGAPp190	RNAi[a]	*BL31070*	−	TRiP line, VALIUM1
tum	RNAi[a]	*BL35007*	−	TRiP line, VALIUM20
CdGAPr	RNAi[a]	*BL38279*	−	TRiP line, VALIUM20
Ocrl	RNAi[a]	*BL34722*	−	TRiP line, VALIUM20
RhoGAP18B	RNAi[a]	*BL31165*	−	TRiP line, VALIUM20
Graf	RNAi[a]	*BL31692*	−	TRiP line, VALIUM1
cv-c	RNAi[a]	*BL6443*	−	Billuart et al., 2001
RacGAP84C	not tested			
conu	homozygote	*LL04815*	−	Neisch et al., 2013
Rlip	homozygote	*c02656*	−	Bloomington
RhoGEF				
Sos	RNAi[a]	*BL34833*	−	TRiP line, VALIUM20
RtGEF	RNAi[a]	*BL32947*	−	TRiP line, VALIUM20
CG10188	RNAi[a]	*BL33047*	−	TRiP line, VALIUM20
CG42674	RNAi[a]	*BL34943*	−	TRiP line, VALIUM20
Exn	RNAi[a]	*BL33373*	−	TRiP line, VALIUM20
GEFmeso	RNAi[a]	*BL42545*	−	TRiP line, VALIUM20
Trio	RNAi[a]	*BL43549*	++	TRiP line, VALIUM20
Trio	MARCM	*E4.1*	++	Awasaki et al., 2000
Unc-89	RNAi[a]	*BL34000*	−	TRiP line, VALIUM20
Vav	RNAi[a]	*BL39059*	−	TRiP line, VALIUM20
CG43658	RNAi[a]	*BL32341*	−	TRiP line, VALIUM20
CG30456	RNAi[a]	*BL34380*	−	TRiP line, VALIUM20
pbl	RNAi[a]	*BL28343*	−	TRiP line, VALIUM10
sif	RNAi[a]	*BL25789*	−	TRiP line, VALIUM10
Zir	RNAi[a]	*BL28005*	−	TRiP line, VALIUM10
Cdep	RNAi[a]	*BL31168*	−	TRiP line, VALIUM1
CG15611	RNAi[a]	*BL31158*	−	TRiP line, VALIUM1
CG30440	RNAi[a]	*BL31207*	−	TRiP line, VALIUM1
CG33275	RNAi[a]	*BL31221*	−	TRiP line, VALIUM1
CG7397	RNAi[a]	*7397R-1*	−	NIG-FLY
CG7397	RNAi[a]	*7397R-2*	+	NIG-FLY
RhoGAP1A	RNAi[a]	*BL33390*	−	TRiP line, VALIUM20
RhoGEF2	RNAi[a]	*BL34643*	+	TRiP line, VALIUM20
RhoGEF2	MARCM	*4.1*	−	Barrett et al., 1997
RhoGEF3	RNAi[a]	*BL42526*	−	TRiP line, VALIUM20
RhoGEF4	RNAi[a]	*BL42550*	+	TRiP line, VALIUM20
RhoGEF4	RNAi[a]	*BL31178*	−	TRiP line, VALIUM1
RhoGEF4	RNAi[a]	*8606R-1*	−	NIG-FLY
RhoGEF4	RNAi[a]	*8606R-2*	−	NIG-FLY
RhoGEF64C	RNAi[a]	*BL31130*	−	TRiP line, VALIUM1

[a]The UAS-RNAi stocks were driven by *ppk-GAL4, UAS-mCD8GFP, UAS-dcr2*.

[b]v'C4da neurons did not survive to the adult stage.

++, moderate; +, weak; -, none

At least 3 neurons for each genotype were analyzed.